Landauovy hladiny

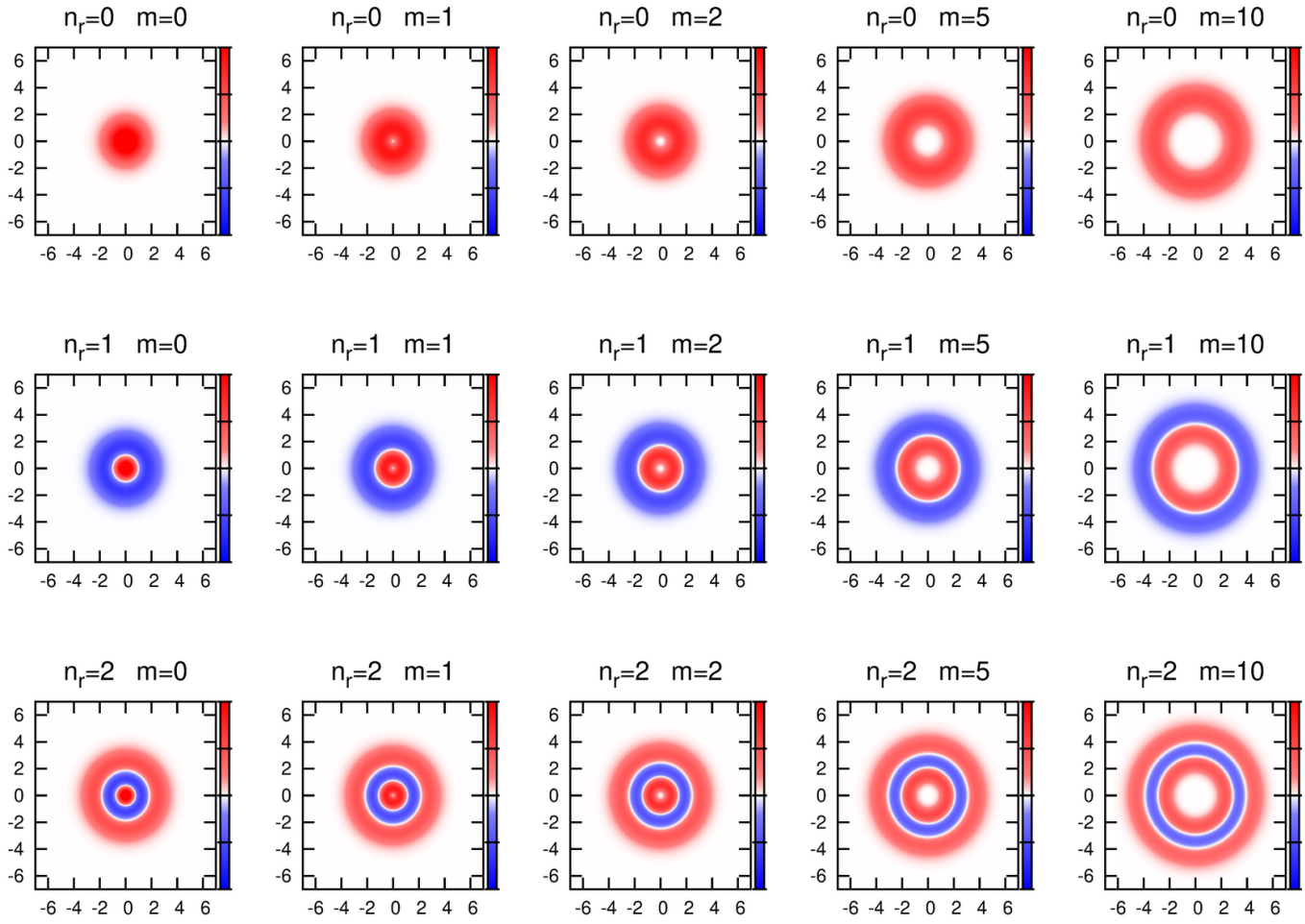

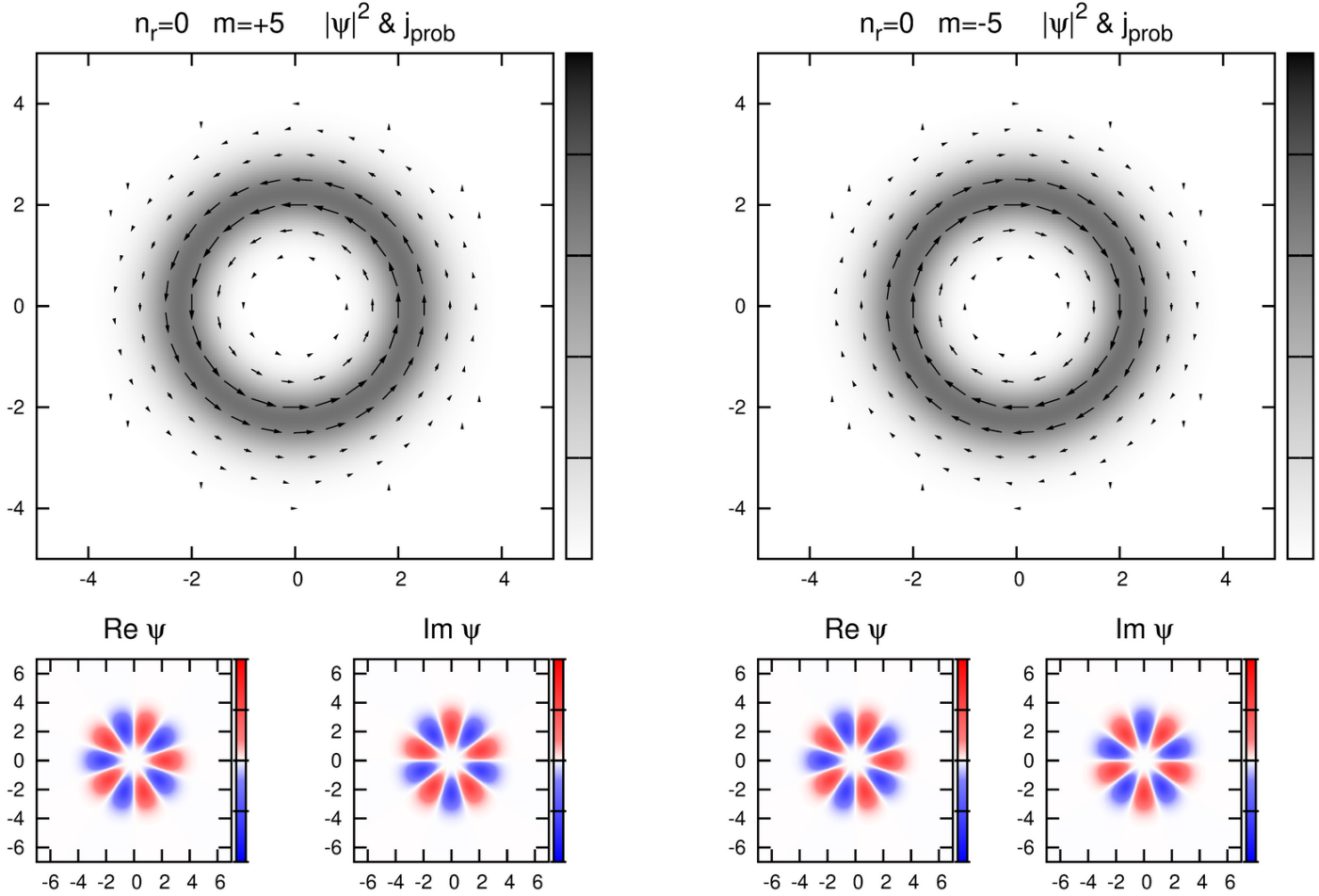
n_r=0 m=+5 $|\psi|^2$ & j_{prob}
n_r=0 m=-5 $|\psi|^2$ & j_{prob}
Re ψ
Im ψ
Re ψ
Im ψ

Landauovy hladiny viděné v transportním experimentu

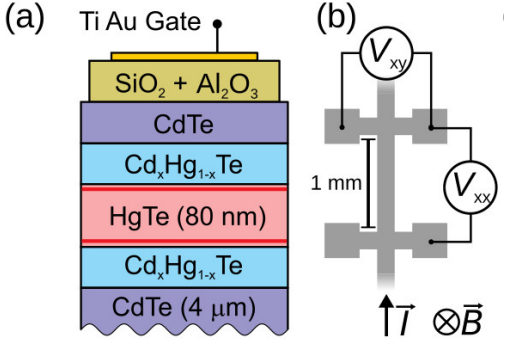

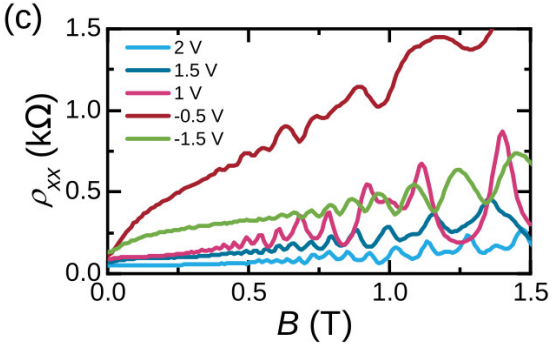

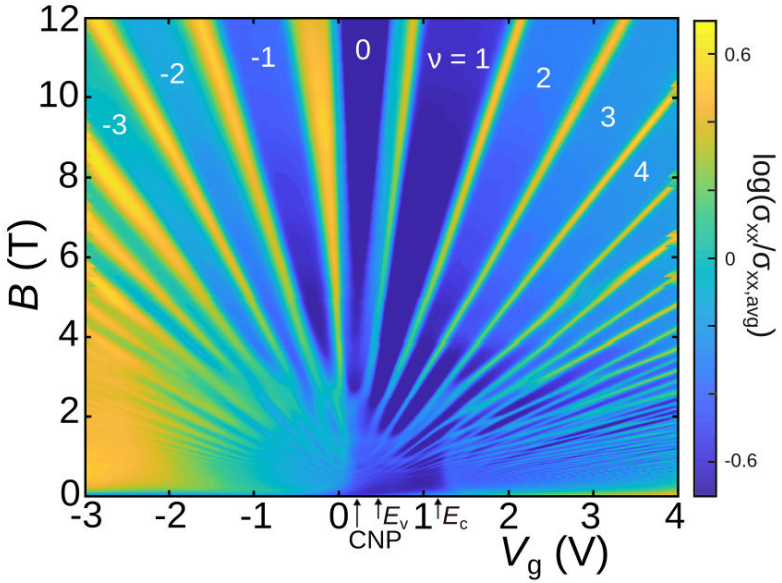

Landauovy hladiny $E_n \sim B\left(n+\frac{1}{2}\right)$

Ziegler et al., Phys. Rev. Res. 2, 033003 (2020)

Landauovy hladiny viděné v optickém experimentu

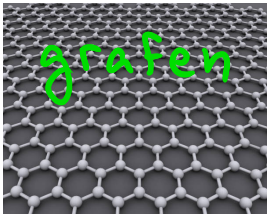

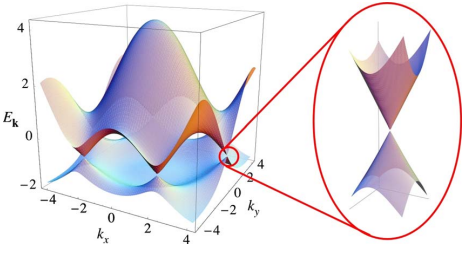

disperzní relace se liší od $E_k = \frac{\hbar^2 k^2}{2m}$

Landauovy hladiny $E_n \sim \sqrt{Bn}$

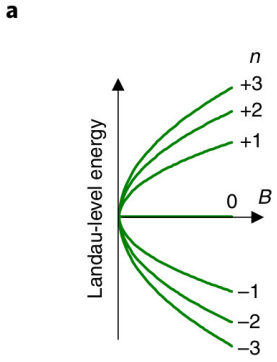

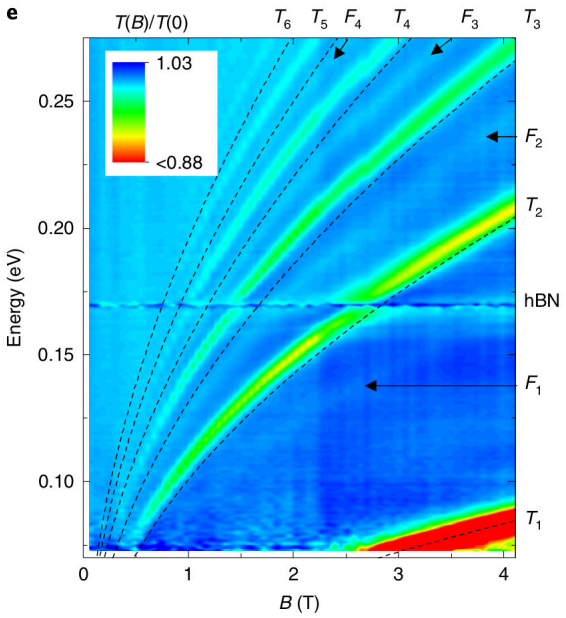

přechody

$\hbar\omega = E_n - E_{n-1}$

Nedoliuk et al., Nature Nanotechnology 14, 756 (2019)

Starkův jev v lithiu

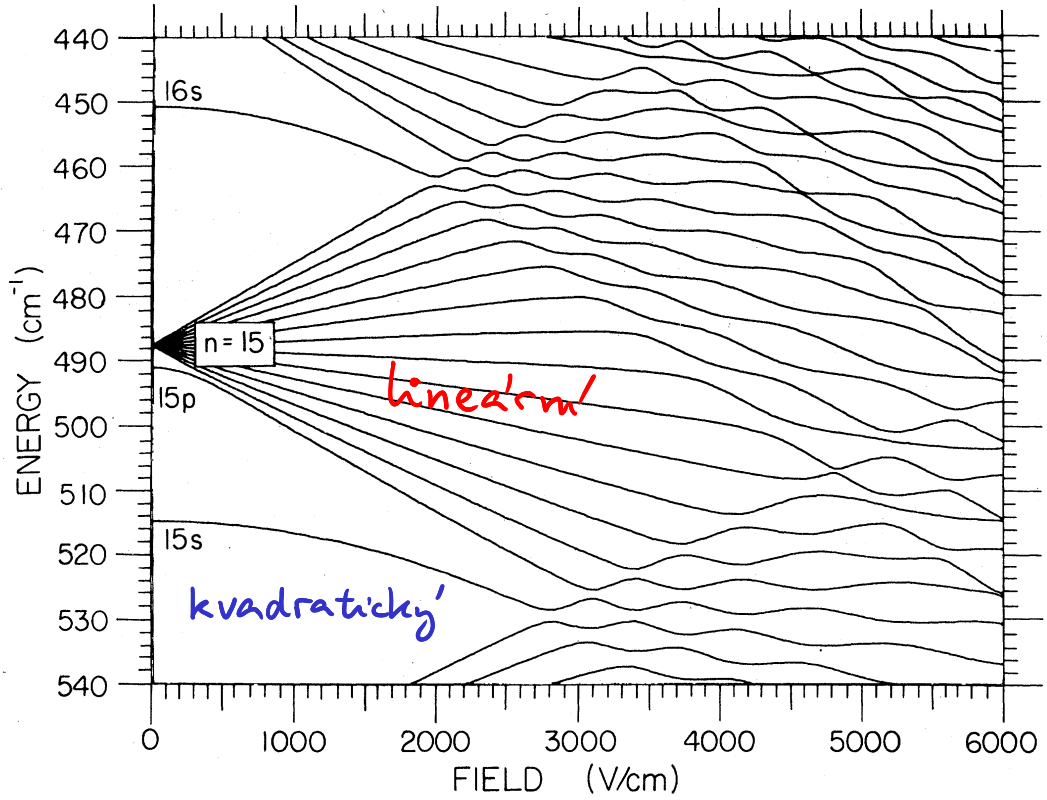

FIG. 6. Lithium, $m = 0$.

Zimmerman et al., Phys. Rev. A 20, 2251 (1979)

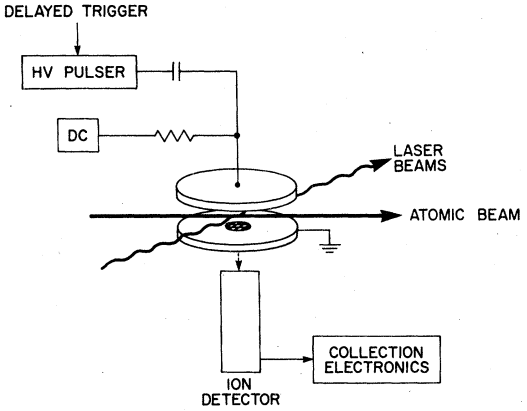

FIG. 2. Experimental arrangement.

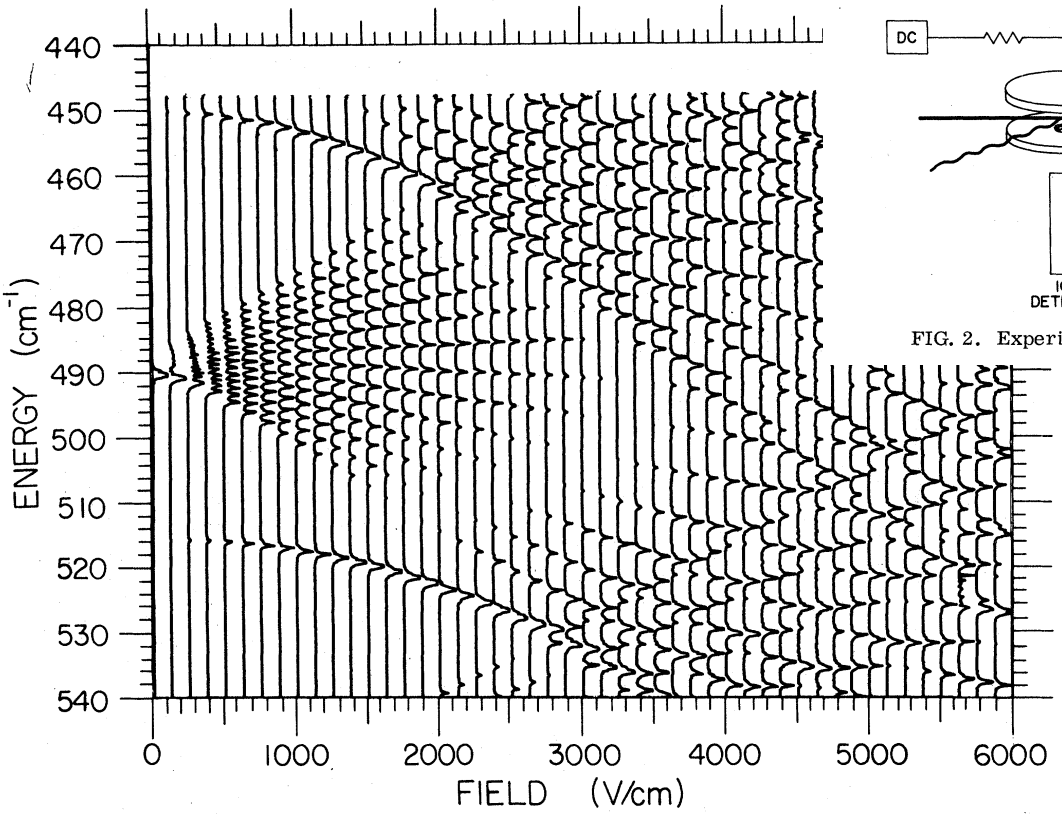

FIG. 7. Lithium, $m = 0$; experimental Stark structure.

Zimmerman et al., Phys. Rev. A 20, 2251 (1979)

Zeemanův jev a solární magnetogramy

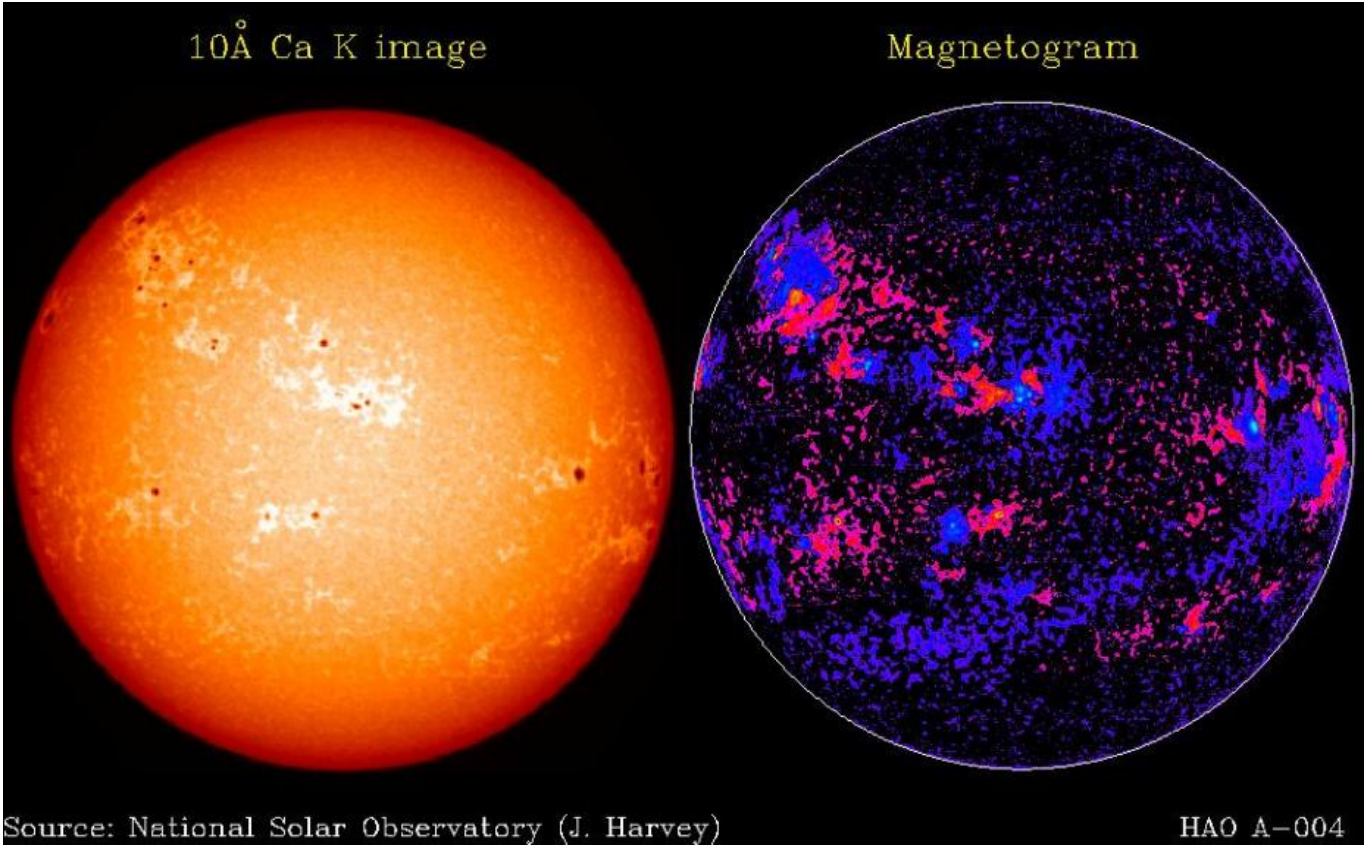

Sternův-Gerlachův experiment

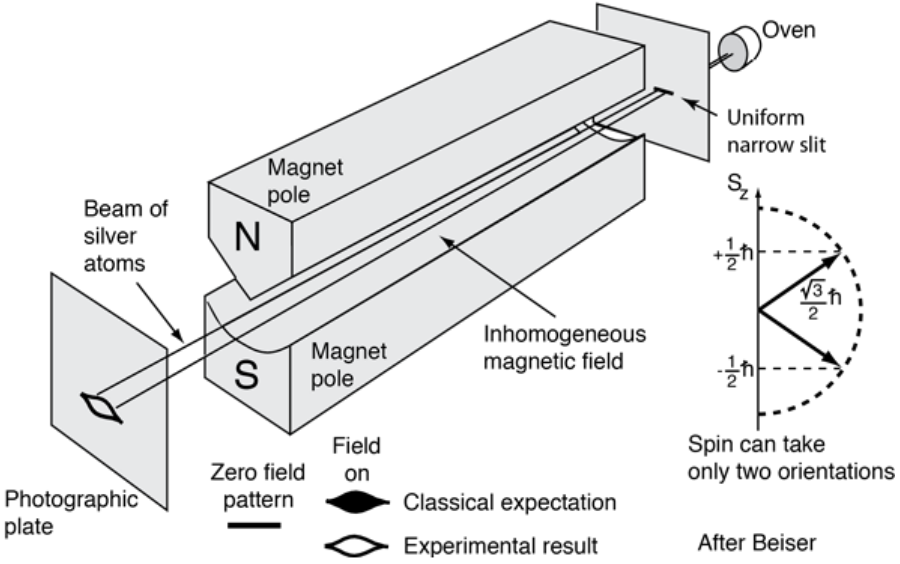

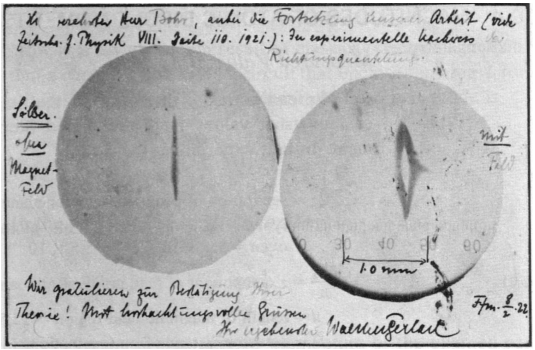

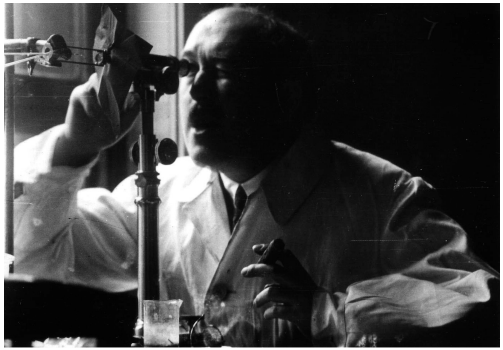

Blochova sféra

$$|\chi\rangle = c_1|\uparrow\rangle + c_2|\downarrow\rangle$$

$$= \cos\frac{\vartheta}{2}|\uparrow\rangle + e^{i\varphi}\sin\frac{\vartheta}{2}|\downarrow\rangle$$

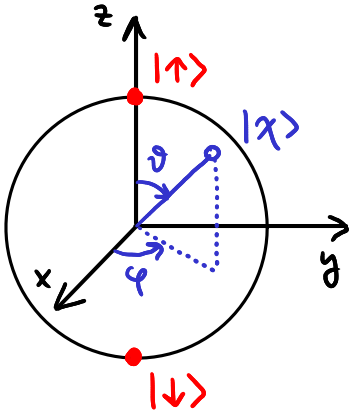

normovanost automaticky: $|c_1|^2 + |c_2|^2 = 1$

celková fáze vynechána: ~~$e^{i\alpha}$~~ $\left(\cos\frac{\vartheta}{2}|\uparrow\rangle + e^{i\varphi}\sin\frac{\vartheta}{2}|\downarrow\rangle\right)$

střední hodnoty komponent spinu:

$$\langle S_x\rangle = \frac{\hbar}{2}\langle\hat{G}_x\rangle = \frac{\hbar}{2}\begin{pmatrix}c_1^* & c_2^*\end{pmatrix}\begin{pmatrix}0 & 1\\ 1 & 0\end{pmatrix}\begin{pmatrix}c_1\\ c_2\end{pmatrix} = \frac{\hbar}{2}(c_2^*c_1 + c_1^*c_2) = \frac{\hbar}{2}\sin\vartheta\cos\varphi$$

$$\langle S_y\rangle = \frac{\hbar}{2}\langle\hat{G}_y\rangle = \frac{\hbar}{2}\begin{pmatrix}c_1^* & c_2^*\end{pmatrix}\begin{pmatrix}0 & -i\\ i & 0\end{pmatrix}\begin{pmatrix}c_1\\ c_2\end{pmatrix} = \frac{\hbar}{2}i(c_2^*c_1 - c_1^*c_2) = \frac{\hbar}{2}\sin\vartheta\sin\varphi$$

$$\langle S_z\rangle = \frac{\hbar}{2}\langle\hat{G}_z\rangle = \frac{\hbar}{2}\begin{pmatrix}c_1^* & c_2^*\end{pmatrix}\begin{pmatrix}1 & 0\\ 0 & -1\end{pmatrix}\begin{pmatrix}c_1\\ c_2\end{pmatrix} = \frac{\hbar}{2}(|c_1|^2 - |c_2|^2) = \frac{\hbar}{2}\cos\vartheta$$

NMR - Nukleární magnetická rezonance

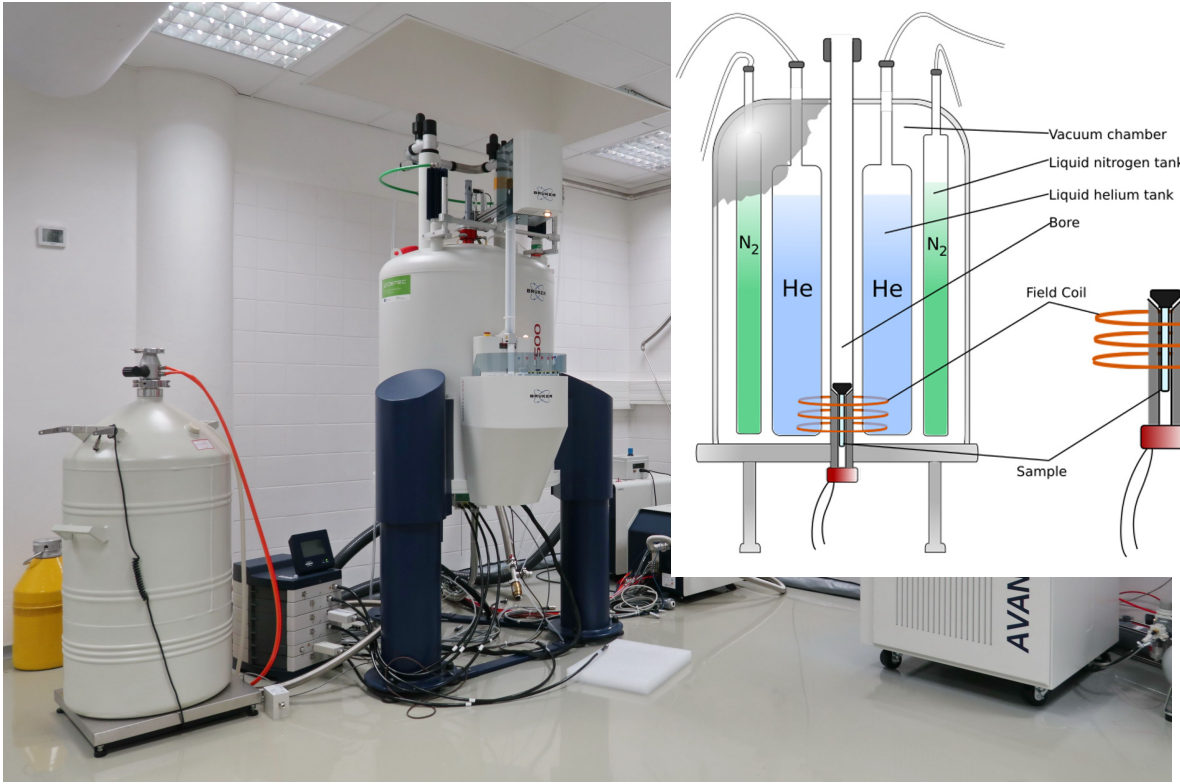

https://nmr.ceitec.cz/equipment/

Odhalování struktury biomolekul pomocí NMR

nature structural & molecular biology

ARTICLES

https://doi.org/10.1038/s41594-020-0489-2

Atomic-resolution structure of HIV-1 capsid tubes by magic-angle spinning NMR

Manman Lu[1,2,3], Ryan W. Russell[1,2], Alexander J. Bryer[1,2], Caitlin M. Quinn[1], Guangjin Hou[1,5], Huilan Zhang[1], Charles D. Schwieters[4], Juan R. Perilla[1,2]✉, Angela M. Gronenborn[2,3]✉ and Tatyana Polenova[1,2]✉

HIV-1 capsid plays multiple key roles in viral replication, and inhibition of capsid assembly is an attractive target for therapeutic intervention. Here, we report the atomic-resolution structure of capsid protein (CA) tubes, determined by magic-angle spinning NMR and data-guided molecular dynamics simulations. Functionally important regions, including the NTD β-hairpin, the cyclophilin A-binding loop, residues in the hexamer central pore, and the NTD-CTD linker region, are well defined. The structure of individual CA chains, their arrangement in the pseudo-hexameric units of the tube and the inter-hexamer interfaces are consistent with those in intact capsids and substantially different from the organization in crystal structures, which feature flat hexamers. The inherent curvature in the CA tubes is controlled by conformational variability of residues in the linker region and of dimer and trimer interfaces. The present structure reveals atomic-level detail in capsid architecture and provides important guidance for the design of novel capsid inhibitors.

[1]Department of Chemistry and Biochemistry, University of Delaware, Newark, DE, USA. [2]Pittsburgh Center for HIV Protein Interactions, University of Pittsburgh School of Medicine, Pittsburgh, PA, USA. [3]Department of Structural Biology, University of Pittsburgh School of Medicine, Pittsburgh, PA, USA. [4]Imaging Sciences Laboratory, Center for Information Technology, National Institutes of Health, Bethesda, MD, USA. [5]Present address: State Key Laboratory of Catalysis, Dalian Institute of Chemical Physics, The Chinese Academy of Sciences, Dalian, P. R. China. ✉e-mail: jperilla@udel.edu; amg100@pitt.edu; tpolenov@udel.edu

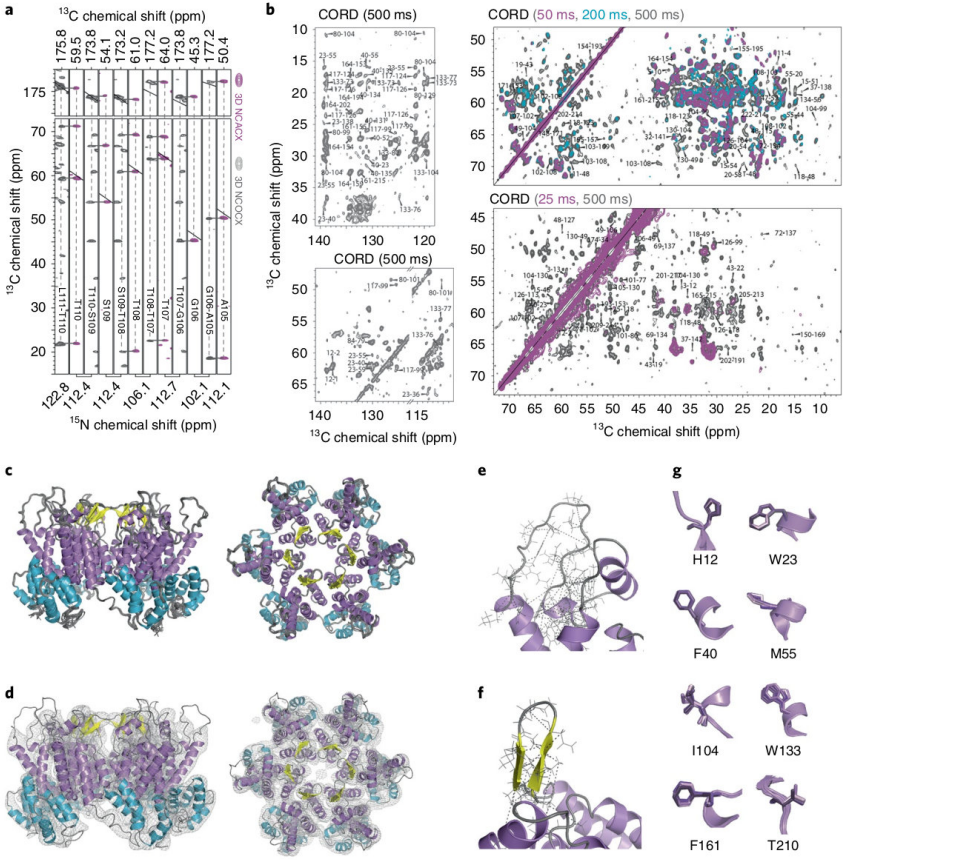

Fig. 1 | MAS-NMR spectra and structure of the hexameric unit in CA tubular assemblies. a, Representative strips extracted from 3D NCACX (magenta) and NCOCX (dark gray) spectra of U-^{13}C,^{15}N-enriched CA tubular assemblies, illustrating sequential assignments for residues 105–110. **b**, Superposition of selected regions of 2D CORD spectra of [1,6-^{13}C-glucose,U-^{15}N]-CA (top) and [2-^{13}C-glucose,U-^{15}N]-CA (lower) samples for different mixing times: 25 ms and 50 ms, magenta; 200 ms, teal; 500 ms, gray. Unambiguous correlations are labeled by amino acid number in the sequence. **c**, Side and top views of the final ensemble of the 10 lowest-energy structures of the CA hexamer unit in the tubular CA assembly. **d**, Side and top views of the superposition of the lowest-energy structure of the NMR-derived CA hexamer unit and the 8-Å resolution cryo-EM density map. **e**,**f**, Details of the MAS-NMR-derived distance restraint network for the CypA loop and the β-hairpin, respectively. **g**, Selected side chain conformations in the final ten-conformer ensemble.

MRI - Magnetic Resonance Imaging